AFRL-VS-TR-2003-1606

COMPUTING SURFACE CHARGING IN THE AURORAL ENVIRONMENT USING NASCAP-2K

V.A. Davis
M.J. Mandell
G.A. Jongeward

Science Applications International Corporation
10260 Campus Point Drive
San Diego, CA 92121

May 2003

Scientific Report No. 3

AIR FORCE RESEARCH LABORATORY
Space Vehicles Directorate
29 Randolph Rd.
AIR FORCE MATERIEL COMMAND
Hanscom AFB, MA 01731-3010

This technical report has been reviewed and is approved for publication.

/Signed/
DAVID COOKE
Contract Manager

/Signed/
ROBERT MORRIS
Branch Chief

This document has been reviewed by the ESC Public Affairs Office and has been approved for release to the National Technical Information Service.

Qualified requestors may obtain additional copies form the Defense Technical Information Center (DTIC). All others should apply to the National Technical Information Service.

If your address has changed, if you with to be removed from the mailing list, or if the addressee is no longer employed by your organization, please notify AFRL/VSIM, 29 Randolph Rd., Hanscom AFB, MA 01731-3010. This will assist us in maintaining a current mailing list.

Do not return copies of this report unless contractual obligations or notices on a specific document require that it be returned.

REPORT DOCUMENTATION PAGE

Form Approved
OMB No. 0704-0188

1. REPORT DATE *(DD-MM-YYYY)*	2. REPORT TYPE	3. DATES COVERED *(From - To)*
01-05-2004	SCIENTIFIC REPORT NO. 3	

4. TITLE AND SUBTITLE
Computing Surface Charging in the Auroral Environment Using Nascap 2k

5a. CONTRACT NUMBER
F19628-98-C-0074

5b. GRANT NUMBER

5c. PROGRAM ELEMENT NUMBER
63401F

6. AUTHOR(S)
V. A. Davis, M. J. Mandell, and G. A. Jongeward

5d. PROJECT NUMBER
2822

5e. TASK NUMBER
GC

5f. WORK UNIT NUMBER
MX

7. PERFORMING ORGANIZATION NAME(S) AND ADDRESS(ES)
Science Applications International Corporation
10260 Campus Point Drive
San Diego, CA 92121

8. PERFORMING ORGANIZATION REPORT NUMBER
SAIC 03/2032

9. SPONSORING/MONITORING AGENCY NAME(S) AND ADDRESS(ES)
Air Force Research Laboratory
29 Randolph Road
Hanscom AFB, MA 01731-3010

10. SPONSOR/MONITOR'S ACRONYM(S)
AFRL/VSBX

11. SPONSOR/MONITOR'S REPORT NUMBER(S)
AFRL-VS-2003-1606

12. DISTRIBUTION/AVAILABILITY STATEMENT
Approved for Public Release; Distribution Unlimited.

13. SUPPLEMENTARY NOTES

14. ABSTRACT

At high latitudes, during periods of auroral activity, low-earth polar orbiting spacecraft can pass through a region of intense, energetic electron fluxes and low thermal plasma density. The Nascap-2k computer code has been extended to model spacecraft surface charging in the auroral region. This report documents how to use the new capabilities, the equations used to describe the environment and its interactions with the surfaces, and the validation of the results.

15. SUBJECT TERMS
Spacecraft Charging Space Environment Aurora
Plasma

16. SECURITY CLASSIFICATION OF:			17. LIMITATION OF ABSTRACT	18. NUMBER OF PAGES	19a. NAME OF RESPONSIBLE PERSON
a. REPORT	b. ABSTRACT	c. THIS PAGE			David Cooke
UNCLASS	UNCLASS	UNCLASS	SAR	38	19b. TELEPHONE NUMBER *(Include area code)* 781-377-2931

TABLE OF CONTENTS

FIGURES

TABLE

1. INTRODUCTION

This report describes the auroral spacecraft charging model implemented in the Nascap-2k spacecraft charging computer code. Drs. Victoria A. Davis and Myron J. Mandell developed and implemented the flux and charging models, with some assistance from Gary A. Jongeward with the auroral environmental flux model. The use of the Nascap-2k auroral charging model is described in Chapter 2. The formulas used to describe the surface fluxes are given in Chapters 3 through 7. Chapter 8 compares the results of sample calculations with those computed using other auroral spacecraft charging codes.

2. USING NASCAP-2K

Choosing "Polar" Orbit and "Surface Charging" Problem Type on the Problem tab (Figure 1) specifies spacecraft charging calculations using an auroral environment. The charging currents can be computed using either "Analytic Currents" (a strictly analytic description of the currents described in the sections *Incident electron flux* and *Analytic model of incident ion flux* below) or "Analytic Electron & Tracked Ion Currents" (where the electron current is computed analytically and the ion current is computed by particle tracking). Ion currents from particle tracking require "Potentials in Space" and "Surface Currents" calculations. Space potentials can be computed with either "Analytic Space Charge" or "Self-consistent with Ion Trajectories." Only the low energy component of the plasma is used in the computation of space charge, as the high energy electrons contribute only a low density of order 10^6 m^{-3}.

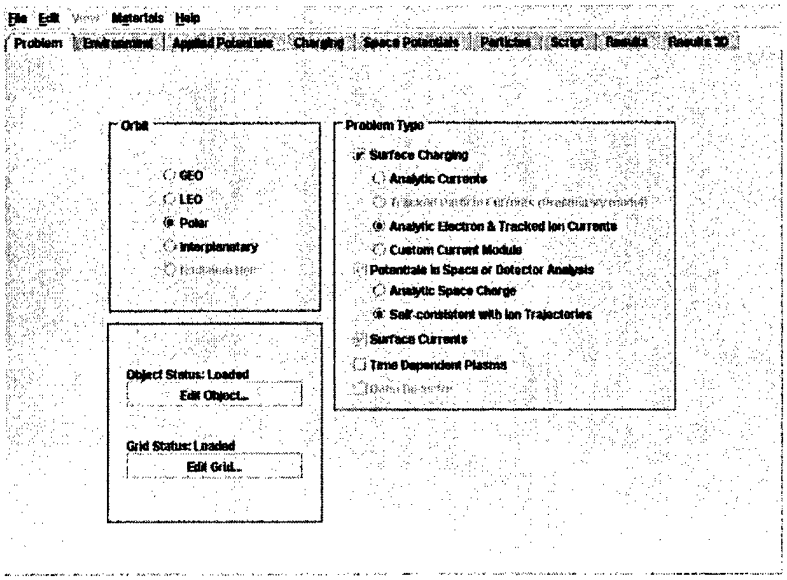

Figure 1. Problem Tab for an Auroral Charging Calculation with the Charge Density Computed From Tracked Ions and Barometric Electrons.

The components of the environment are specified on the Environment Tab. (Figure 2)

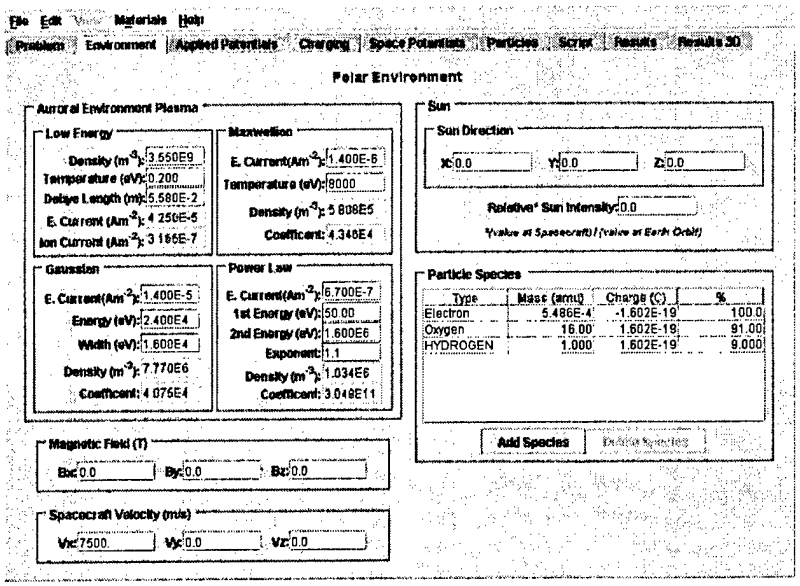

Figure 2. Environment Tab for Auroral Charging.

Only species with positive charge are used in the computation of the tracked ion flux component. If the space potentials are computed with analytic space charge, the ion flux is computed using the parameters given on the "Surface Currents" subtab of the "Particles" tab. If the space potentials are computed self-consistently with ion trajectories, the ion flux is computed using the parameters given on the "Ion Densities" subtab (Figure 3) of the "Particles" tab.

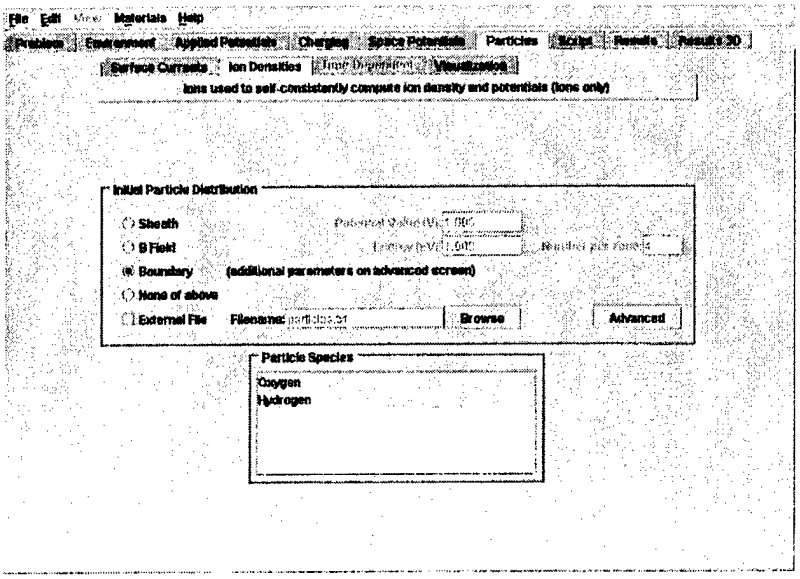

Figure 3. Ion Densities Subtab of the Particles Tab.

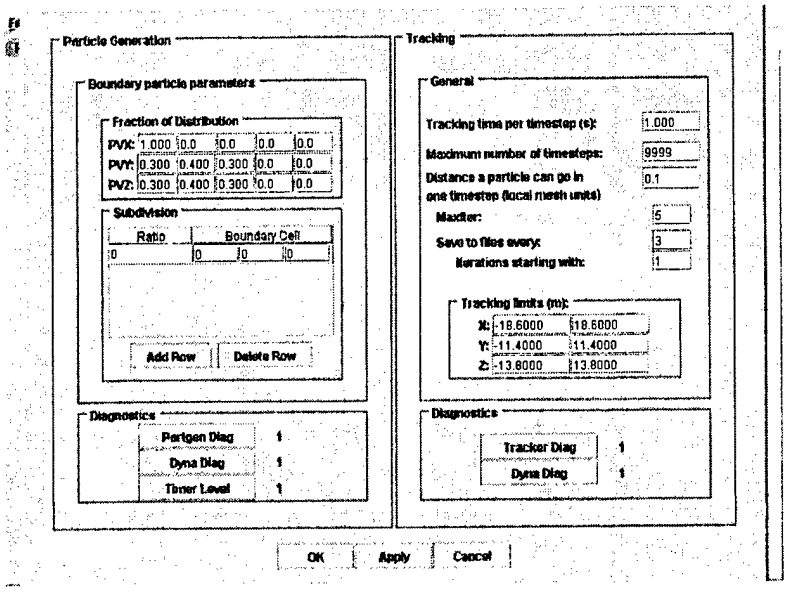

Figure 4. Advanced Screen of the Particles Tab. Calculations Self-Consistent with Ion Densities Require Extra Particles Created Either as a Thermal Distribution or by Subdivision.

The initial potentials are specified in the same way as for geosynchronous charging calculations.

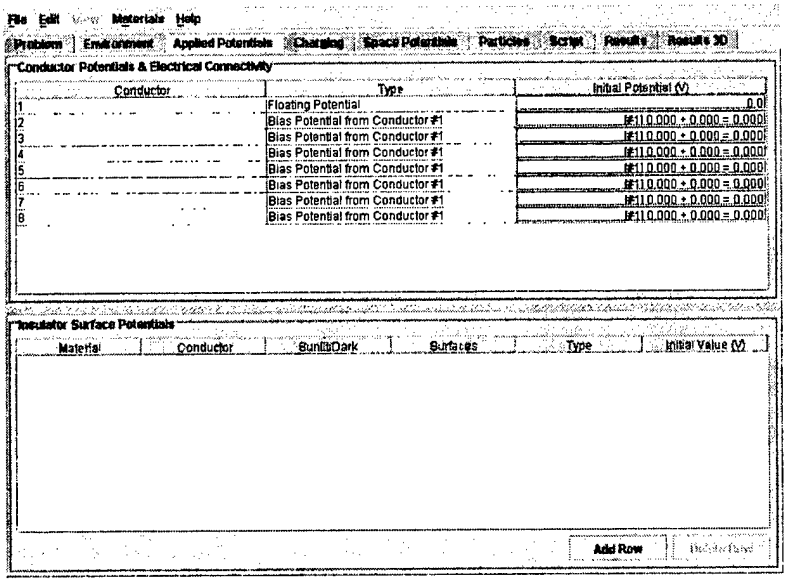

Figure 5. Initial Potentials Tab.

The charging timesteps are specified on the charging tab (Figure 6) in the same way as for a geosynchronous charging calculation. Computing surface charging self-consistently with tracked ions is an iterative calculation. In this case, the number of iterations is given in the Iteration box on the Space Potentials Tab (Figure 7) and the number of timesteps on the Charging tab is ignored. One timestep is used per iteration.

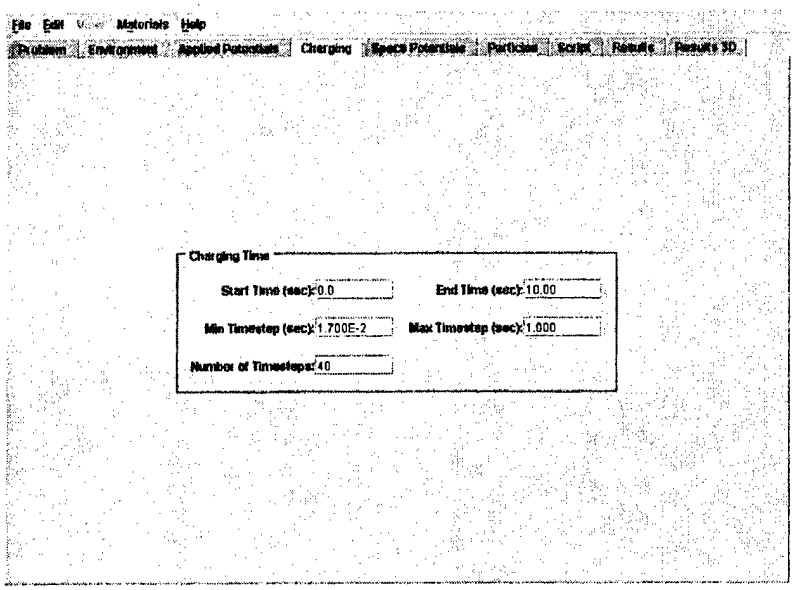

Figure 6. Charging Tab.

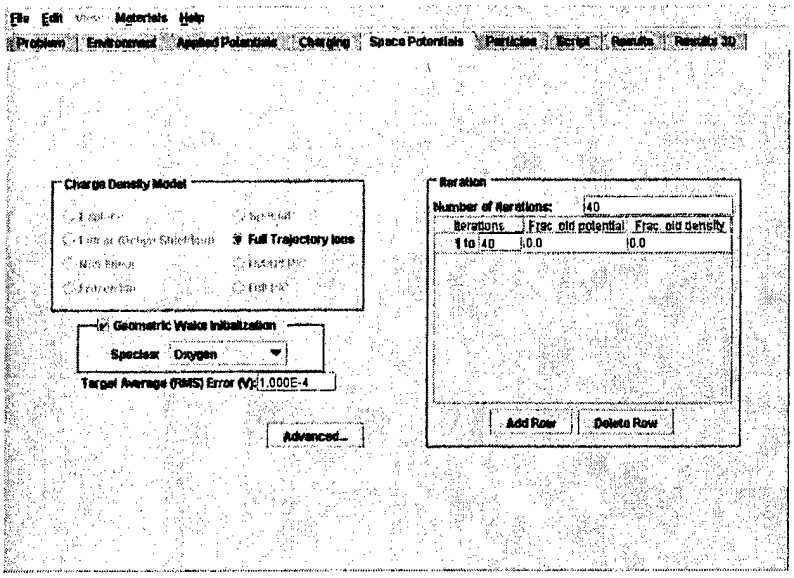

Figure 7. Space Potentials Tab. Auroral Charging Calculations Using Tracked Ions Use the Iteration Parameters in the Space Potentials and Ion Density(Self-Consistent Ions Only) Calculations.

The script used to specify an auroral charging calculation with "Analytic Currents" is the same as the script used to specify a geosynchronous charging calculation except for the environment definition. The script used to specify an auroral charging calculation with "Analytic Electron & Tracked Ion Currents" is similar to that for a LEO surface charging calculation using "Tracked Particle Currents." The calculation is initialized with "Charge Surfaces," "Potentials in Space," "Create Particles," and "Track Particles," commands. The sequence is repeated "Number of Iterations" times, ending with a "Potentials in Space" command. For "Self-consistent with Ion Trajectories" charge densities, the "Traj_Ion" command is included in the sequence before each

"Potentials in Space" command after the first one. The first Charge Surfaces command has the same subcommands as an "Analytic Currents" calculation, except the "DoOneTimeStep" subcommand is used in place of the "DoTimeSteps" subcommand. A "UseTrackedIons" subcommand specifies that the most recent tracked surface current values are to be used as the ion flux. A "FieldsFromFile" subcommand specifies that the electric fields used to compute the suppression of secondary electrons and photoelectrons are to be read from the database rather than computed by the BEM module. The BEM module assumes no space charge, while the Potentials in Space module of Nascap-2k (which writes its results into the database) computes electric fields using the specified model for space charge.

3. INCIDENT ELECTRON FLUX

All species of the low energy plasma are described by a Maxwellian distribution. The high energy electrons are described by a Fontheim distribution, which has three components, specified by the net current in each component. The Maxwellian component describes a broad electron distribution, the Gaussian component describes the "inverted-V" part of the spectrum, and the Power Law component describes the secondary and backscattered electrons from interactions between the Gaussian beam and the rest of the plasma. The Power Law component only contributes at energies between specified lower and upper cutoffs. The effective density of each component is the expectation value of the distribution function.
The electron differential flux ($m^{-2}\ s^{-1}\ eV^{-1}$) is specified by

$$\text{Flux}(E) = \sqrt{\frac{e}{2\pi\theta m_e}}\frac{E}{\theta} n \exp\left(-\frac{E}{\theta}\right) + \pi\zeta_{max} E \exp\left(-\frac{E}{\theta_{max}}\right) + \pi\zeta_{gauss} E \exp\left(-\left(\frac{E_{gauss}-E}{\Delta}\right)^2\right) + \pi\zeta_{power} E^{-\alpha} \quad (1)$$

where n and θ are the density and temperature of the low energy ionospheric plasma, e and m_e are the electron charge and mass, and the ζs, θ_{max}, E_{gauss}, Δ, and α are constants. Figure 8 shows the electron flux for an auroral environment.

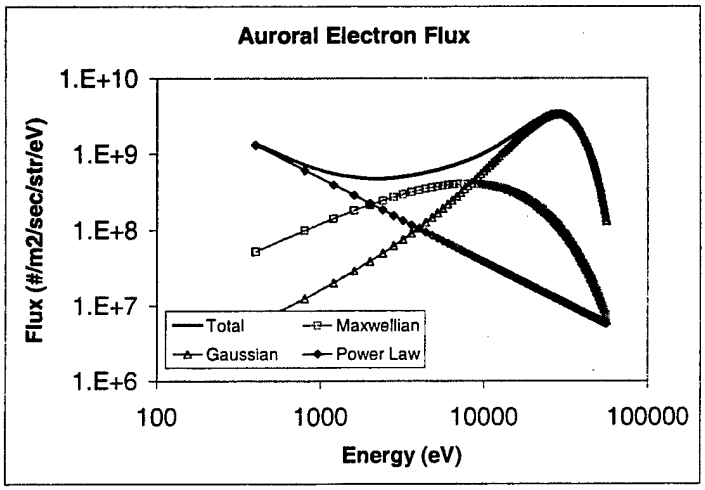

Figure 8. Fontheim Electron Spectrum Using Parameters Shown in Figure 2.

4. ANALYTIC MODEL OF INCIDENT ION FLUX

The ion flux density to each surface is assumed to be the orbit-limited ion flux density to a point on a uniform potential sphere at the same angle relative to the ram direction. The orbit-limited assumption, which is appropriate to tenuous plasma conditions where the Debye length is tens to hundreds of meters, is questionable in the auroral case for which the Debye length may be of order 10 cm. Also, the spherical geometry approximation may be less valid here than for tenuous plasma environments. Nonetheless, use of this model provides a means of obtaining at least qualitative results without the effort and uncertainties associated with particle tracking.
We next derive the equations for ion collection by a negatively charged conducting sphere of radius a in a flowing plasma with ion temperature T. We determine the current density as a function of angle. All velocities are in units of the plasma thermal velocity

$$V_T = (kT/M)^{1/2} \tag{2}$$

where k is Boltzman's constant and M is the ion mass. Energies are measured in units of kT, so that energy conservation for an ion at the surface of an attracting sphere is expressed by

$$\frac{1}{2}v^2 - \Phi = E = \frac{1}{2}v_0^2 \tag{3}$$

where v is the velocity of the ion, Φ the potential energy of the ion at the surface of the sphere, E the total energy of the ion, and v_0 the speed of the ion at an infinite distance from the sphere. The normal current density at a point on the sphere where the unit outward normal is **n** and is given by

$$j = j(\mathbf{n}) = \iiint \mathbf{v}\cdot\mathbf{n}\ f_0(\mathbf{v_0})d^3\mathbf{v} \tag{4}$$

where f_0 is the plasma velocity space distribution function and the integration variable is the negative of the impact velocity at the surface. In the rest frame of the sphere

$$f_0(\mathbf{v_0}) = (2\pi)^{-3/2}\exp\left(-\frac{1}{2}(\mathbf{v_0}-\mathbf{V_0})^2\right) \tag{5}$$

where $\mathbf{V_0}$ is the flow velocity of the plasma.

Now introduce a coordinate system (Figure 9) whose z axis lies in the direction of the normal to the sphere at the point where we wish to calculate j. Let the x-z plane be determined by this normal and the plasma flow velocity and let φ be the azimuthal angle between the x-z plane and the orbital plane of an ion. The angle between the surface normal and the flow velocity is ξ. A particle launched at the sphere surface with polar angle α has polar angle θ_∞ at $r = \infty$.

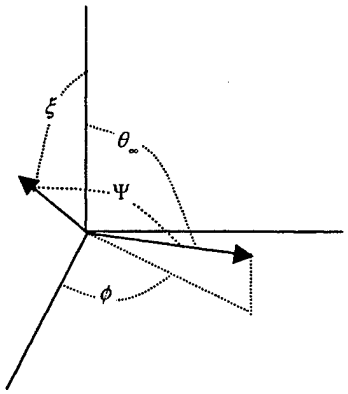

Figure 9. Coordinates Used in the Drifting Maxwellian Ion Current Calculation.

The current j may now be written

$$j = (2\pi)^{-3/2} \int_0^{\infty} dv_0 \int_0^{\pi/2} d\alpha \int_0^{2\pi} d\varphi \; v_0 \left(v_0^2 + 2\Phi\right) \times \exp\left(-\frac{1}{2}\left(v_0^2 - 2v_0 V_0 \cos\psi + V_0^2\right)\right) \times \cos\alpha \sin\alpha \quad (6)$$

where α is the polar angle of the reverse trajectory ion launched from the sphere and ψ is the angle between the flow vector and the incident velocity at infinity associated through the dynamics with the angle α.

Referring to Figure 9, we have

$$\cos\psi = \cos\xi\cos\theta_\infty + \sin\xi\sin\theta_\infty\cos\varphi \quad (7)$$

Integration over the azimuth yields

$$j = (2\pi)^{-3/2} \int_0^{\infty} v_0 (v_0^2 + 2\Phi) \exp(-v_0^2/2) \; F(v_0) \; dv_0 \quad (8)$$

where

$$F(v_0) = 2\pi \int_0^{\pi/2} \exp\left(-V_0^2/2\right) \exp\left(v_0 V_0 \cos\xi\cos\theta_\infty\right) \times I_0\left(v_0 V_0 \sin\xi\sin\theta_\infty\right) \cos\alpha\sin\alpha \, d\alpha \quad (9)$$

and $I_0(x)$ is the modified Bessel function of zero order

$$I_0(x) = \frac{1}{2\pi} \int_0^{2\pi} \exp(-x\cos\varphi) d\varphi \quad (10)$$

The angles at infinity are functions of the launch angle and the energy. The required relations are determined from the orbit relations in a 1/r potential:

$$\frac{a}{r}=\frac{\Phi}{2(E+\Phi)\sin^2\alpha}\times\left(1+\sqrt{1+\frac{4E(E+\Phi)}{\Phi^2}\sin^2\alpha}\cos(\theta-\theta_0)\right) \tag{11}$$

Measuring orbital angles from the polar axis that is normal to the sphere at the launch point and setting a = r determines the angle θ_0,

$$\cos\theta_0=\left(2\left(\frac{E}{\Phi}+1\right)\sin^2\alpha-1\right)\sqrt{1+\frac{4E(E+\Phi)}{\Phi^2}\sin^2\alpha}^{-1} \tag{12}$$

Setting $r=\infty$ gives

$$\cos(\theta_\infty-\theta_0)=-\sqrt{1+\frac{4E(E+\Phi)}{\Phi^2}\sin^2\alpha}^{-1} \tag{13}$$

The velocity and angle integrals are done numerically. Figure 10 shows the flux density to a low-potential sphere, illustrating the progression from uniform flux a low Mach number to cos θ on the ramward side and zero on the wake side for high Mach number. Figure 11 shows the flux density to a high-potential sphere, showing that the flux decreases with ion energy (more or less as [1-V/E]) and is fairly uniform over the sphere, even at realistic Mach numbers.

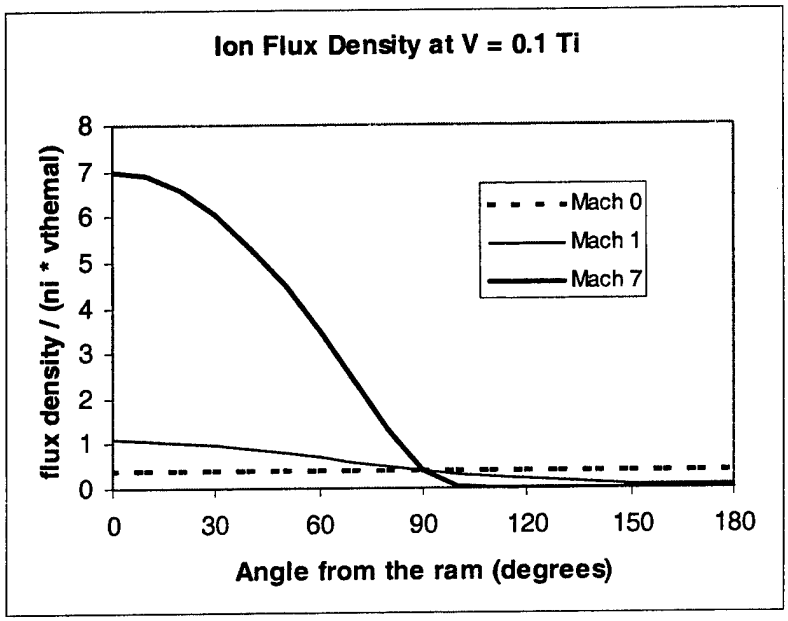

Figure 10. Relative Ion Currents at Low Sphere Potentials.

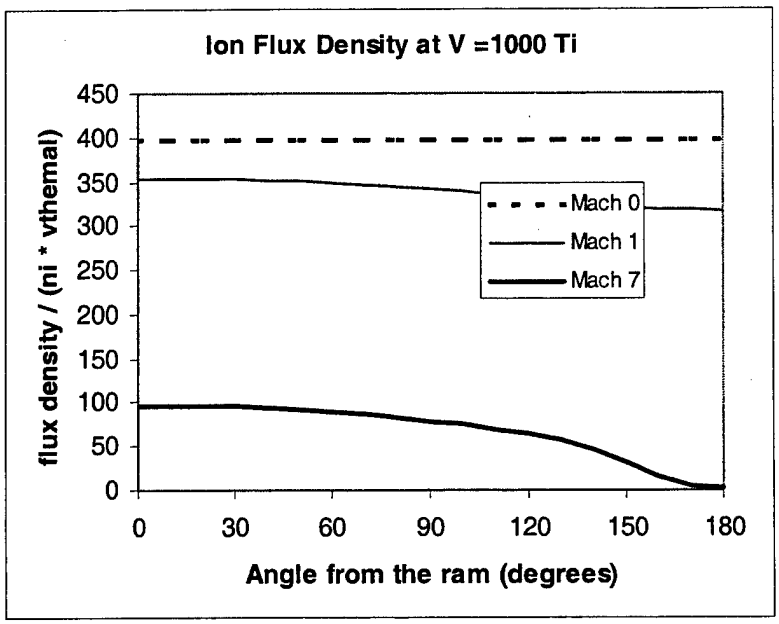

Figure 11.Relative Ion Currents at About 100 V in the Ionosphere.

5. SECONDARY AND BACKSCATTERED ELECTRON FLUXES

The secondary and backscattered electron fluxes are computed for each component of the incident current separately.

The secondary and backscattered electron fluxes due to the Maxwellian components of the incident electron fluxes (low energy and Fontheim) are computed in the same manner as for a geosynchronous Maxwellian plasma.

The secondary and backscattered electron fluxes due to the Gaussian and Power Law components of the incident electron flux are computed by integrating the products of the distribution functions and the yield functions as is done for the Maxwellian components. The yield for the Maxwellian and Power Law components is taken to be that for isotropically incident flux. The yield for the Gaussian component is taken to be that for normally incident flux. The techniques for doing the integrals are given below.

The secondary electron flux due to the incident ion flux when the incident ion flux is computed using the analytic orbit limited model is the sum over the species of the integral of the product of the incident ion flux times the average yield for a cosine theta distribution of ions with an energy of $\frac{1}{2}MV_0^2 - e\phi$, where M is the ion mass, V_o is the ram velocity, and ϕ is the surface potential. The rate of secondary emission is assumed to be independent of mass (except indirectly through the incident velocity). If no species are specified on the Environment Tab, the plasma is assumed to be 100 percent of ions of mass 16 times the proton mass.

The secondary electron flux due to the incident ion flux when the incident ion flux is computed by particle tracking is the tracked ion current times the yield. The secondary yield is given by a normally incident ion with kinetic energy of $\frac{1}{2}MV_0^2 - e\phi$, where M is 16 atomic mass units, V_0 is the ram velocity, and ϕ is the surface potential.

6. PARTIAL DENSITIES AND COEFFICIENTS

The partial densities shown on the Environment Tab are given by the expressions below. The techniques used to compute the average values of the square root of the inverse of the energy are given in the section on integrals below.

$$\text{Density}_{max} = \pi e \zeta_{max} \theta_{max}^2 \frac{4}{e}\sqrt{\frac{m_e}{2e}}\left\langle\sqrt{\frac{1}{E}}\right\rangle^{max} \tag{14}$$

$$\text{Density}_{gauss} = \pi e \zeta_{gauss} \Delta \frac{1}{2}\left(\Delta \exp\left(-\left(\frac{E_o}{\Delta}\right)^2\right) + E_o\sqrt{\pi}\ \text{erfc}\left(-\frac{E_o}{\Delta}\right)\right) \times \frac{4}{e}\sqrt{\frac{m_e}{2e}}\left\langle\sqrt{\frac{1}{E}}\right\rangle^{gauss} \tag{15}$$

$$\text{Density}_{power} = \pi e \zeta_{power} \frac{1}{\alpha - 1}\left(\frac{1}{(E_1)^{\alpha-1}} - \frac{1}{(E_2)^{\alpha-1}}\right) \times \frac{4}{e}\sqrt{\frac{m_e}{2e}}\left\langle\sqrt{\frac{1}{E}}\right\rangle^{power} \tag{16}$$

The coefficients shown on the Environment Tab are given by the expressions below.

$$\zeta_{max} = \frac{I_{max}}{\pi e \theta_{max}^2} \tag{17}$$

$$\zeta_{gauss} = \frac{I_{gauss}}{\pi e \Delta \frac{1}{2}\left(\Delta \exp\left(-\left(\frac{E_o}{\Delta}\right)^2\right) + E_o\sqrt{\pi}\left(1 + \text{erf}\left(\frac{E_o}{\Delta}\right)\right)\right)} \tag{18}$$

$$\zeta_{power} = \frac{I_{power}}{\pi e}(\alpha - 1)\left(\frac{1}{E_1^{\alpha-1}} - \frac{1}{E_2^{\alpha-1}}\right)^{-1} \tag{19}$$

7. INTEGRALS

The technique used to compute the average value of the yield or other quantity over the distribution is given in this section.

7.1 Average Value of Y(E) for Maxwellian

$$\langle Y \rangle^{max} = \frac{\int_{max(0,\phi_{surf})}^{\infty} Y(E) E \exp\left(-\frac{E-\phi_{surf}}{\theta_e}\right) dE}{\int_{max(0,\phi_{surf})}^{\infty} E \exp\left(-\frac{E-\phi_{surf}}{\theta_e}\right) dE} \tag{20}$$

(If for ions, use ϕ_{surf} rather than $-\phi_{surf}$)
To compute the numerator use

Normalization

$$\int_{max(0,\phi_{surf})}^{\infty} E \exp\left(-\frac{E-\phi_{surf}}{\theta_e}\right) dE \tag{21}$$

If $\phi_{surf} >= 0$, then

$$= \theta \int_0^1 (-\theta \ln u + \phi_{surf}) du = -\theta^2 \int_0^1 (\ln u) du + \theta\phi_{surf} = \theta^2 + \theta\phi_{surf} = \theta^2 \left(1 + \frac{\phi_{surf}}{\theta}\right)$$

If $\phi_{surf} < 0$, then

$$= -\theta^2 \exp\left(\frac{\phi_{surf}}{\theta}\right) \int_0^1 (\ln u) du = \theta^2 \tag{22}$$

7.2 Average Value of Y(E) for Gaussian Term

$$\langle Y \rangle^{gauss} = \frac{\int_{max(0,\phi_{surf})}^{\infty} Y(E) E \exp\left(-\left(\frac{E-E_{gauss}-\phi_{surf}}{\Delta}\right)^2\right) dE}{\int_{max(0,\phi_{surf})}^{\infty} E \exp\left(-\left(\frac{E-E_{gauss}-\phi_{surf}}{\Delta}\right)^2\right) dE} \tag{23}$$

$$\int_{\max(0,\phi_{surf})}^{\infty} Y(E)\,E\exp\left(-\left(\frac{E+E_{gauss}-\phi_{surf}}{\Delta}\right)^2\right)dE \qquad \left(\text{substitute } u=\frac{E-E_{gauss}-\phi_{surf}}{\Delta}\right) \tag{24}$$

$$= \int_{\max\left(\frac{-E_{gauss}-\phi_{surf}}{\Delta},\frac{-E_{gauss}}{\Delta}\right)}^{\infty} Y\left(\Delta u+E_{gauss}+\phi_{surf}\right)\left(\Delta u+E_{gauss}+\phi_{surf}\right)\exp\left(-u^2\right)\Delta du$$

(Split into three integrals to isolate the peak.
if $E_{gauss}+\phi_{surf}<0$, the first term in the expansion below is zero and the second term has a different lower limit, and may also be zero.)

$$= \int_{\max\left(\frac{-E_{gauss}-\phi_{surf}}{\Delta},\frac{-E_{gauss}}{\Delta}\right)}^{-\xi} Y\left(\Delta u+E_{gauss}+\phi_{surf}\right)\left(\Delta u+E_{gauss}+\phi_{surf}\right)\exp\left(-u^2\right)\Delta du$$

$$+\int_{-\xi}^{\xi} Y\left(\Delta u+E_{gauss}+\phi_{surf}\right)\left(\Delta u+E_{gauss}+\phi_{surf}\right)\exp\left(-u^2\right)\Delta du \tag{25}$$

$$+\int_{\xi}^{\infty} Y\left(\Delta u+E_{gauss}+\phi_{surf}\right)\left(\Delta u+E_{gauss}+\phi_{surf}\right)\exp\left(-u^2\right)\Delta du$$

$\left(\text{substitute } x=\exp\left(-u^2\right) \text{ and take } \xi \text{ to be small}\right)$

$$\int_{\max(0,\phi_{surf})}^{\infty} Y(E)\,E\exp\left(-\left(\frac{E-E_{gauss}-\phi_{surf}}{\Delta}\right)^2\right)dE \tag{26}$$

$$= \int_{\exp\left(-\left(\min\left(\frac{E_{gauss}+\phi_{surf}}{\Delta},\frac{E_{gauss}}{\Delta}\right)\right)^2\right)}^{\exp\left(-\xi^2\right)} Y\left(\Delta\left(-\sqrt{-\ln x}\right)+E_{gauss}+\phi_{surf}\right)\left(\Delta\left(-\sqrt{-\ln x}\right)+E_{gauss}+\phi_{surf}\right)x\frac{1}{2\sqrt{-\ln x}}\frac{1}{x}\Delta dx$$

$$+Y\left(E_{gauss}+\phi_{surf}\right)\Delta\int_{-\xi}^{\xi}\left(\Delta u+E_{gauss}+\phi_{surf}\right)\exp\left(-u^2\right)du$$

$$+\int_{\exp\left(-\xi^2\right)}^{0} Y\left(\Delta\left(\sqrt{-\ln x}\right)+E_{gauss}+\phi_{surf}\right)\left(\Delta\left(\sqrt{-\ln x}\right)+E_{gauss}+\phi_{surf}\right)x\frac{-1}{2\sqrt{-\ln x}}\frac{1}{x}\Delta dx$$

$$\int_{\max(0,\phi_{surf})}^{\infty} Y(E)\,E\exp\left(-\left(\frac{E-E_{gauss}-\phi_{surf}}{\Delta}\right)^2\right)dE \tag{27}$$

$$=\frac{\Delta}{2}\int_{\exp\left(-\left(\min\left(\frac{E_{gauss}+\phi_{surf}}{\Delta},\frac{E_{gauss}}{\Delta}\right)\right)^2\right)}^{\exp(-\xi^2)} Y\left(-\Delta\sqrt{-\ln x}+E_{gauss}+\phi_{surf}\right)\left(-\Delta+\frac{E_{gauss}+\phi_{surf}}{\sqrt{-\ln x}}\right)dx$$

$$+Y\left(E_{gauss}+\phi_{surf}\right)\Delta\left(E_{gauss}+\phi_{surf}\right)\sqrt{\pi}\,\mathrm{erf}\left(\xi\right)+\frac{\Delta}{2}\int_{0}^{\exp(-\xi^2)} Y\left(\Delta\left(\sqrt{-\ln x}\right)+E_{gauss}+\phi_{surf}\right)\left(\Delta+\frac{E_{gauss}+\phi_{surf}}{\sqrt{-\ln x}}\right)dx$$

Normalization

$$\int_{\max(0,\phi_{surf})}^{\infty} E\exp\left(-\left(\frac{E-E_{gauss}-\phi_{surf}}{\Delta}\right)^2\right)dE \tag{28}$$

$$=\int_{\max\left(\frac{-E_{gauss}-\phi_{surf}}{\Delta},\frac{-E_{gauss}}{\Delta}\right)}^{\infty}\left(\Delta u+E_{gauss}+\phi_{surf}\right)\exp\left(-u^2\right)\Delta du$$

$$=\Delta^2\int_{\max\left(\frac{-E_{gauss}-\phi_{surf}}{\Delta},\frac{-E_{gauss}}{\Delta}\right)}^{\infty} u\exp\left(-u^2\right)du+\Delta\left(E_{gauss}+\phi_{surf}\right)\int_{\max\left(\frac{-E_{gauss}-\phi_{surf}}{\Delta},\frac{-E_{gauss}}{\Delta}\right)}^{\infty}\exp\left(-u^2\right)du$$

$$=\Delta^2\int_{\mathrm{abs}\left(\max\left(\frac{-E_{gauss}-\phi_{surf}}{\Delta},\frac{-E_{gauss}}{\Delta}\right)\right)}^{\infty} u\exp\left(-u^2\right)du+\Delta\left(E_{gauss}+\phi_{surf}\right)\frac{\sqrt{\pi}}{2}\mathrm{erfc}\left(\max\left(\frac{-E_{gauss}-\phi_{surf}}{\Delta},\frac{-E_{gauss}}{\Delta}\right)\right)$$

$$=\frac{\Delta^2}{2}\exp\left(-\min\left(\frac{E_{gauss}+\phi_{surf}}{\Delta},\frac{E_{gauss}}{\Delta}\right)^2\right)+\Delta\left(E_{gauss}+\phi_{surf}\right)\frac{\sqrt{\pi}}{2}\mathrm{erfc}\left(\max\left(\frac{-E_{gauss}-\phi_{surf}}{\Delta},\frac{-E_{gauss}}{\Delta}\right)\right)$$

7.3 Average Value of Y(E) for Power Law:

$$\langle Y\rangle^{power}=\frac{\int_{\max(0,E_1+\phi_{surf})}^{\max(E_2,E_2+\phi_{surf})} Y(E)E\left(E-\phi_{surf}\right)^{-\alpha-1}dE}{\int_{\max(0,E_1+\phi_{surf})}^{\max(E_2,E_2+\phi_{surf})} E\left(E-\phi_{surf}\right)^{-\alpha-1}dE} \tag{29}$$

$$\int_{\max(0,E_1+\phi_{surf})}^{\max(E_2,E_2+\phi_{surf})} E\left(E-\phi_{surf}\right)^{-\alpha-1}dE = \left(-\frac{1}{\alpha-1}\right)\int_{\max(-\phi_{surf},E_1)}^{\max(E_2-\phi_{surf},E_2)^{-\alpha+1}} dz - \phi_{surf}\left(\frac{1}{\alpha}\right)\int_{\max(-\phi_{surf},E_1)}^{\max(E_2-\phi_{surf},E_2)^{-\alpha}} dz \qquad (30)$$

$$= \left(-\frac{1}{\alpha-1}\right)\left(\max\left(E_2-\phi_{surf},E_2\right)^{-\alpha+1} - \max\left(-\phi_{surf},E_1\right)^{-\alpha+1}\right)$$

$$-\phi_{surf}\left(\frac{1}{\alpha}\right)\left(\max\left(E_2-\phi_{surf},E_2\right)^{-\alpha} - \max\left(-\phi_{surf},E_1\right)^{-\alpha}\right)$$

8. VALIDATION OF RESULTS

8.1 Comparison with SEE Spacecraft Charging Handbook

The SEE Spacecraft Charging Handbook gives the following results for a 2 m Kapton cube with orbital speed of 7500 m/s in the x direction. The charging time is 10 s with 40 timesteps. The environment is the "DMSP1" environment shown in Figure 13.

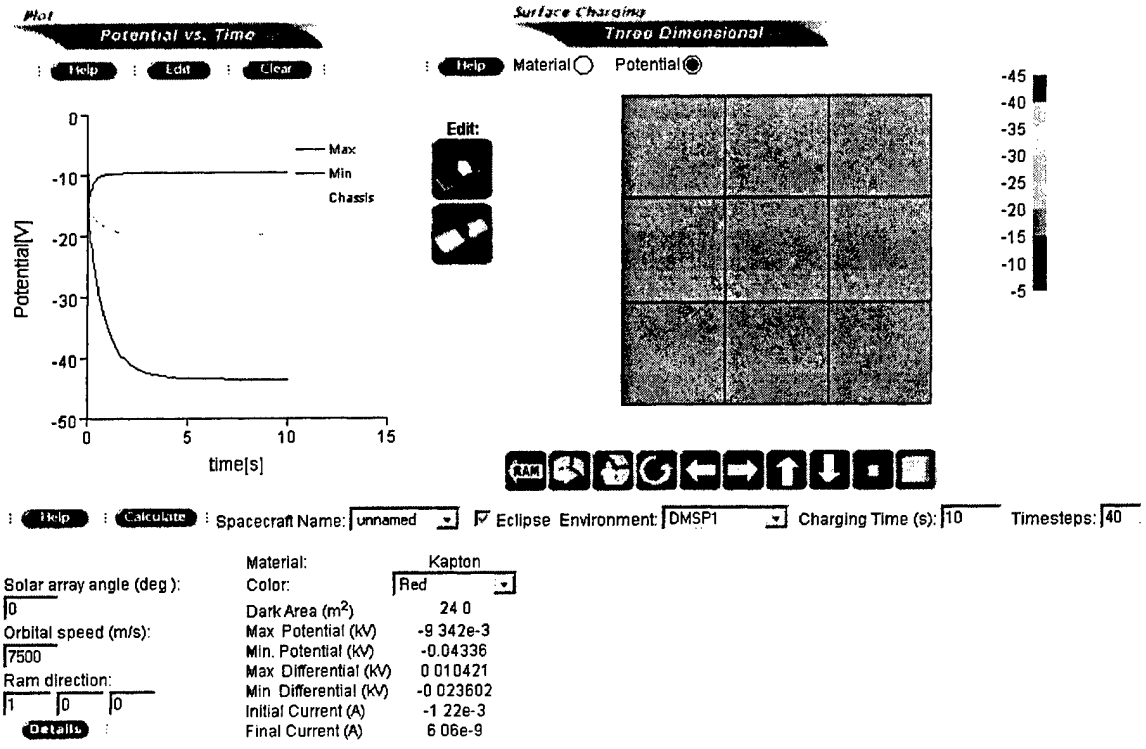

Figure 12. Auroral Charging Test Case as Computed by SEE Spacecraft Charging Handbook.

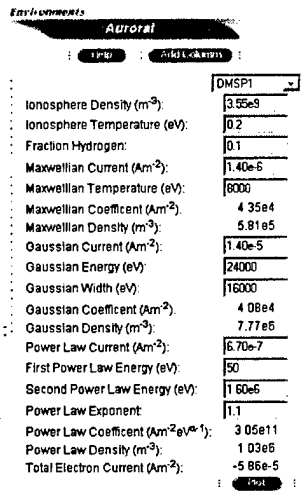

Figure 13. Environment Used for Test Cases.

With a minimum timestep of 0.01 and a maximum timestep of 1 s, the Nascap-2k, Polar, Analytic Currents, charging model gives the same results. For these parameters, this approach gives too little charging. The ion currents are overestimated as Debye screening is ignored.

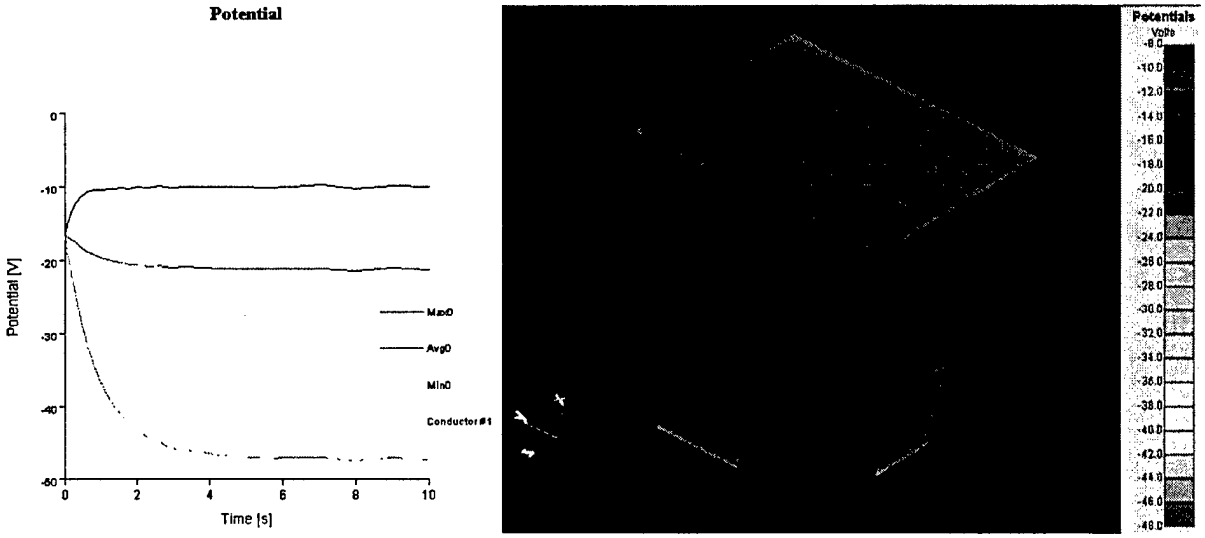

Figure 14. Results From Nascap-2k Test Case Using Environment Currents.

Doing the same problem, but tracking particles in from a sheath (located at -0.277 V) gives more charging as expected, since the orbit limited approximation overestimates the ion current. Three grids were used. The main grid is 24 cubed with a mesh size of 0.8 m. The second grid is also 24 cubed filling the inner eighth of the main grid. The innermost grid is 16 cubed and fills the center of the grid. The results are shown in Figure 15. The highest potential surfaces are along the front edge of the side and the lowest in the back. Figure 16 shows the potential contours around the cube. The cube is moving to the right. Most of the sheath is in the second grid, which has a sheath potential of -0.277 V.

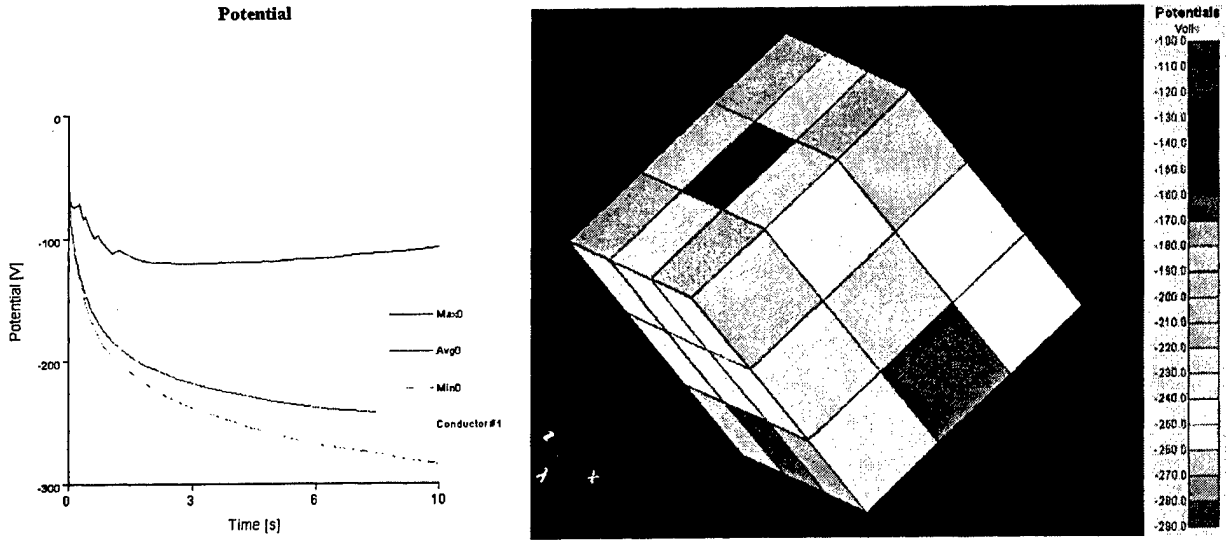

Figure 15. Results From Nascap-2k Test Case Using Tracked Ion Currents. The Top Left Surface is on the Wake Side.

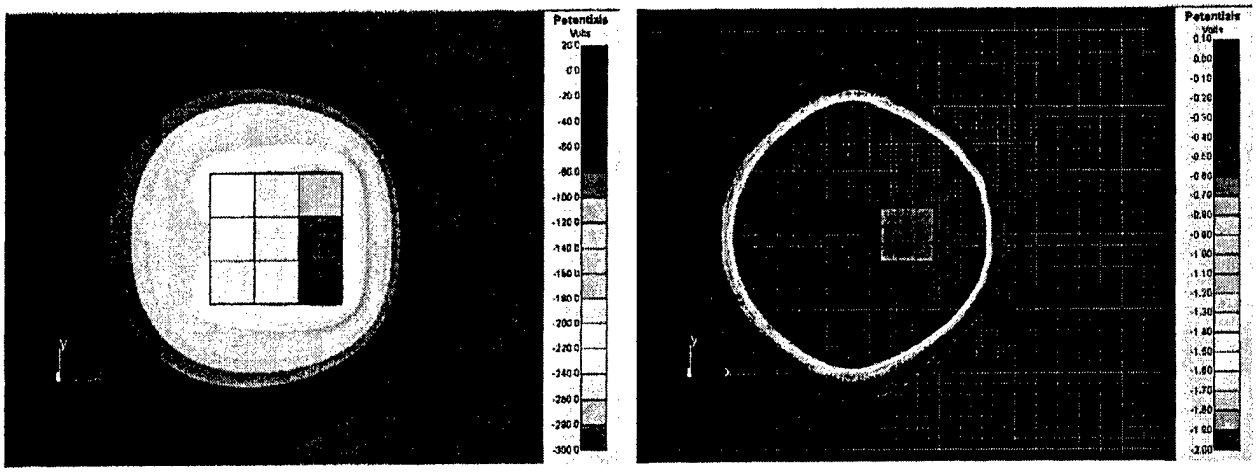

Figure 16. Potential Contours Around Charged Cube with Different Scales.

Repeating the calculation, but computing the charge density using full trajectory ions, gives somewhat lower potentials. Ions with a thermal distribution (1.0 in x; 0.3, 0.4, 0.3 in y; and 0.3, 0.4, 0.3 in z) are tracked from the problem boundaries. The results are shown in Figure 17. The potentials are similar, although more negative. The highest potential is at the back edge of the side.

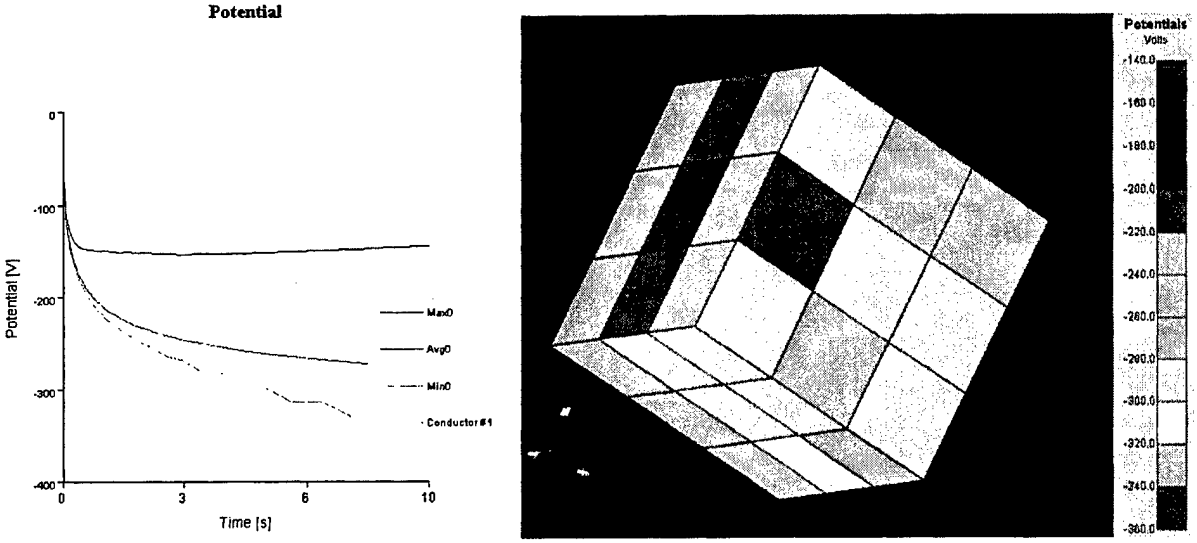

Figure 17. Results From Nascap-2k Test Case Using Tracked Ion Currents and Self-consistent Charge Density. The Top Left Surface is on the Wake Side.

There are two significant differences between the calculation shown in Figure 15 and that shown in Figure 17. The macroparticles tracked are created differently and the charge density is computed differently. In the first case, mono-energetic ions are tracked from a sheath boundary at -0.277 V, while in the second case, a thermal distribution is tracked from the problem boundaries. In the first case the charge density is computed using an analytic formulation and in the second the charge density is computed from the tracked ions and a barometric relation for the electrons. To separate these two effects two additional calculations were done. In the first, the charge density was computed using the analytic formulation and the current computed from a thermal distribution of ions tracked from the problem boundaries. In the second, the charge density was computed using ions tracked from the problem boundary, and the current was computed from ions tracked from a sheath at -0.277 V. The potential time histories are shown in Figure 18. The tracked ion current collected is shown in Figure 19. In all cases, the collected current is roughly linear with chassis potential. The highest current gives the least charging. Both the charge density and the initial macroparticle distribution influence the results. For this particular problem, it is not clear which approach is more correct.

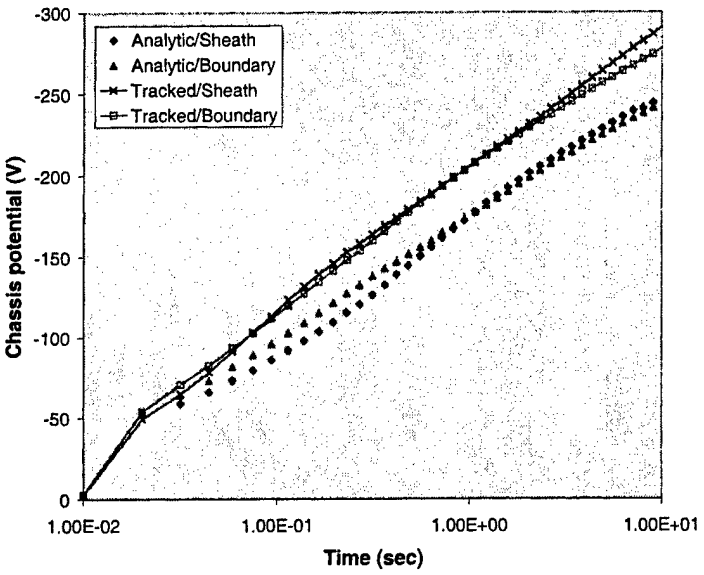

Figure 18. Time History of Potentials for Different Charge Density Formulations and Macroparticle Initial Conditions.

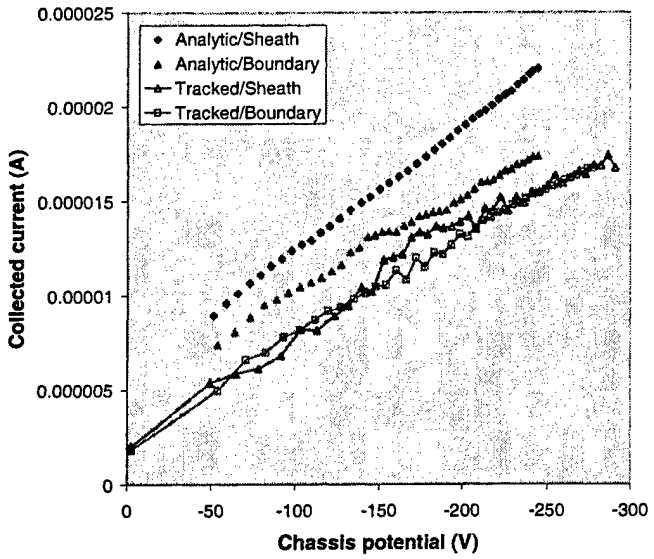

Figure 19. Collected Current as a Function of Chassis Potential (V) for Different Charge Density Formulations and Macroparticle Initial Conditions.

At lower densities, the analytic estimation of the ion current should be more accurate. We did the same calculation with an ambient density two orders of magnitude lower. It is necessary to use a larger grid, so that the entire sheath fits. Changing the outer grid mesh unit to 5 meters, but leaving the grid structure the same, gives a large enough grid. The sheath edge is partially in the outer grid and partially in the second grid. The appropriate sheath potentials are 0.372465 V and 0.147813 V. The calculations were done using the average sheath potential of 0.277 V. At the lower density, the charging occurs faster, so we used 50 timesteps, with a minimum of 0.001s and a maximum of 1 s. The final potentials are shown in Table 1.

Table 1. Final Potentials in Low Density Case.

Case		Potential at 10 s (V)		
Ions	Space charge	Chassis	Maximum	Minimum
Analytic	None	-1257	-1238	-1313
Sheath	Analytic	-1148	-997	-1360
Boundary	Self-consistent	-2393	-2128	-2596

In the Sheath/Analytic space charge case, the most negative potentials are on the wake side and the least negative potentials are on the ram side. In the Boundary/Self-consistent space charge case, the most negative potentials are along the side toward the ram and the least negative potential is on the center surface of the wake side.

Figure 20 shows sample trajectories for the Sheath/Analytic plasma case. Of the trajectories shown, the outer four are undisturbed, the inner two are immediately collected, and the rest loop around the cube one or more times before leaving the computational space.

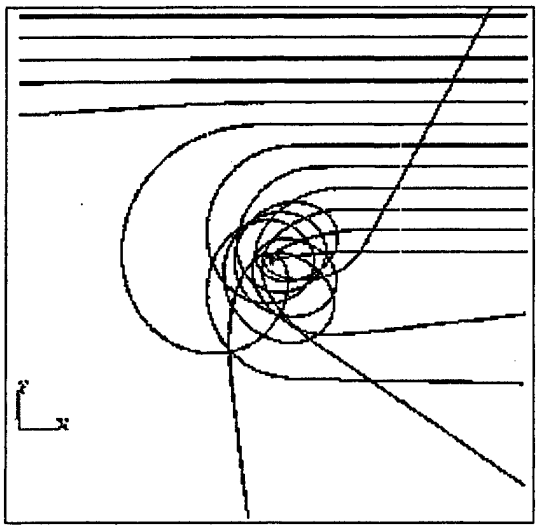

Figure 20. Sample Trajectories for Sheath/Analytic Space Charge Case (Low Density).

Figure 21 shows sample trajectories for the Boundary/Self-consistent plasma case. Of the trajectories shown, the outer six are undisturbed, the inner four are immediately collected, the seventh from the top circles a couple of times are then leaves the computational space, and the eighth from the top provides most of the tangle of trajectory seen before being collected. The trajectories that orbit about the cube before being collected or leaving the computational space provide Debye shielding that decreases the ion current, increasing the charging. The algorithm for computing self-consistent potentials can give potentials that are not as smoothly varying as desired. Better results are often obtained by sharing the potentials or ion densities from iteration to iteration. The parameters for this sharing are set on the Space Potentials Tab. In this case, the space potentials have some non-physical structures that may be numerically reducing the ion energies, leading to higher current collection than physically correct.

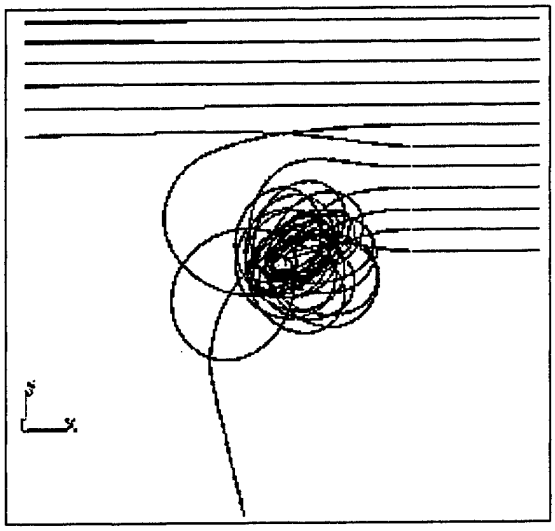

Figure 21. Sample Trajectories for Boundary/Self-Consistent Case (Low Density).

8.2 Comparison with POLAR Results

To validate Nascap-2k we compare the results obtained using Nascap-2k with those obtained using POLAR, which has been validated. The POLAR calculations to which we will compare are given in Reference 1.

We used the POLAR object, which generates some "inconsistent edge" error messages, but is valid. To create the object, we used Nascap/GEO for Windows to create the object, read the Nascap/GEO object into DynaPAC, and then read the DynaPAC object into Object Toolkit.

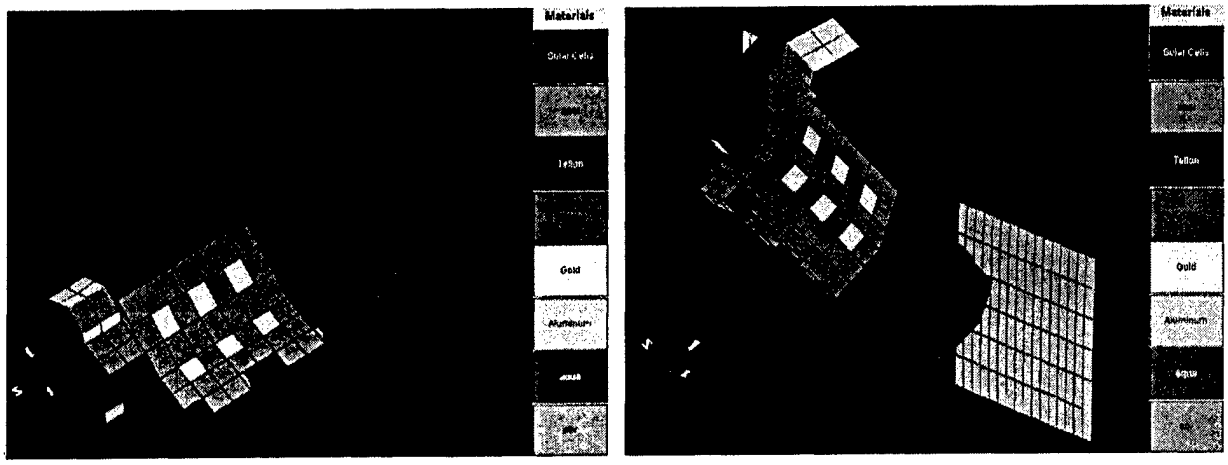

Figure 22. POLAR DMSP Object.

Charging in eclipse from an initial potential of -10 V was computed for a period of 6 s with 45 timesteps varying from 0.0125 s to 0.2 s. In all cases, the charging currents were computed using

an analytic model for the electrons and tracked ions. The charge density was computed either analytically or self-consistently with the ion trajectories. In the first case, the ion currents are computed by tracking macroparticles from the sheath and in the second case by tracking macroparticles from the boundary of the computational space. The environment used is shown in Figure 23.

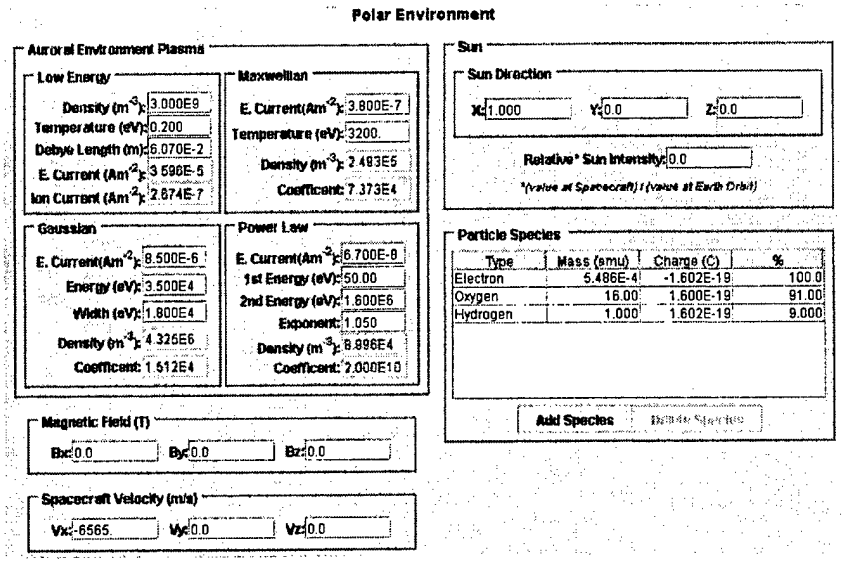

Figure 23. Environment Used for DMSP Charging Calculations.

The results of the calculations are given in Figure 24 through Figure 31. With these choices for parameters, the resulting chassis potential for the analytic charge density case is -707 V and for the self-consistent charge density case is -845 V. In the analytic charge density case the potentials vary between -414 and -888 V; while in the self-consistent charge density case the potentials vary between -710 and -1025 V. The distribution of surface potentials is essentially the same for the two cases, with well-shadowed surfaces the most negative. The chassis rapidly charges to the -400 to 500 V level and continues to charge at about 50 to 60 V per second. With more timesteps, the results might be slightly different.

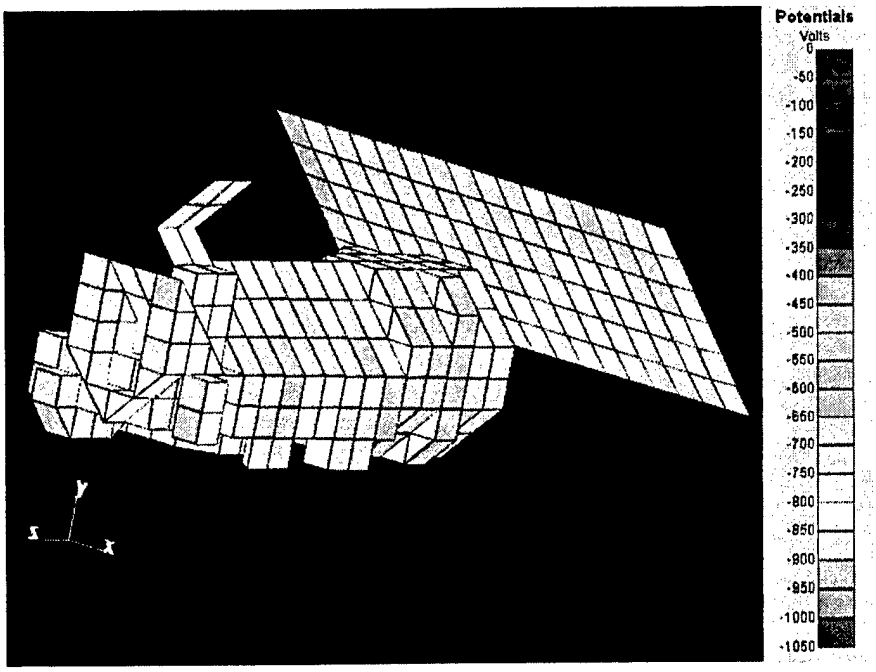

Figure 24. Resulting Surface Potentials for Case with Analytic Charge Density.

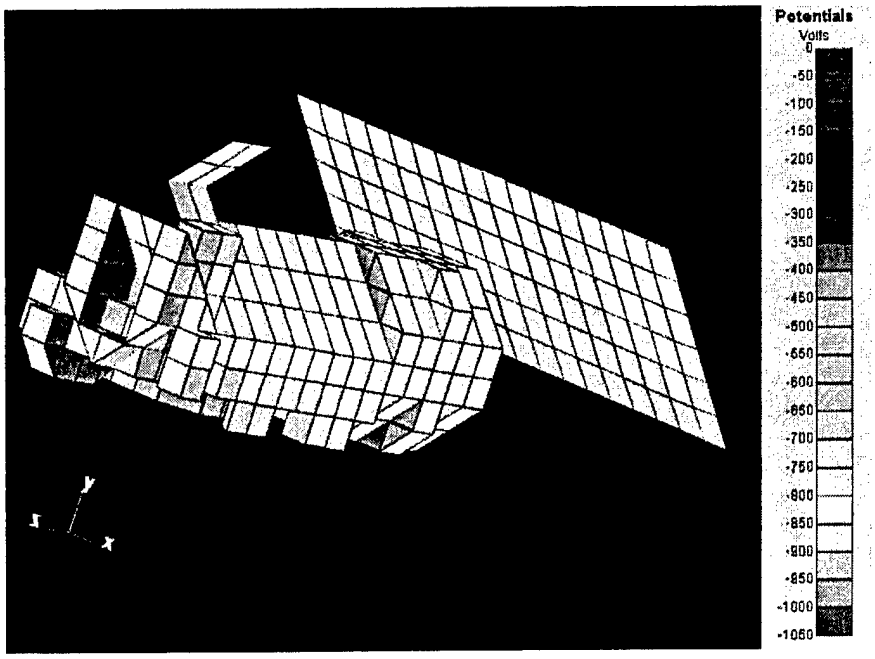

Figure 25. Resulting Surface Potentials for Case with Self-Consistent Charge Density.

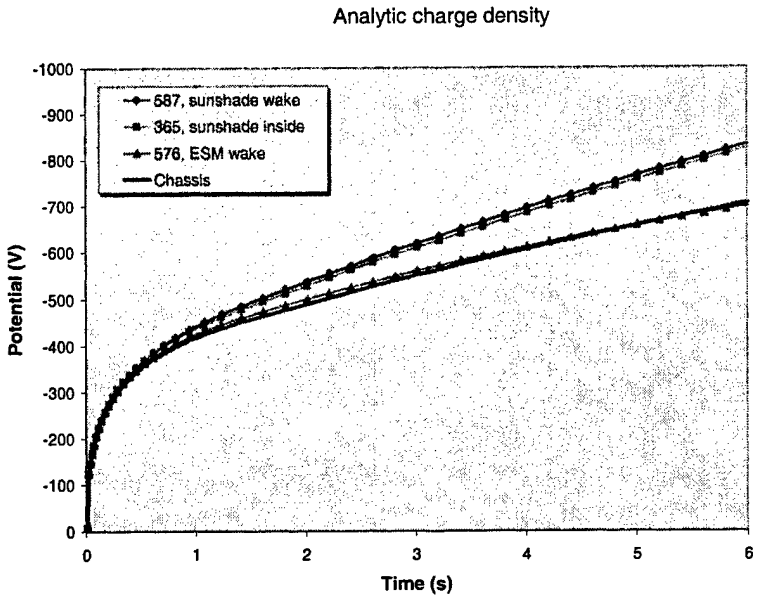

Figure 26. Time History of Charging with Analytic Charge Density.

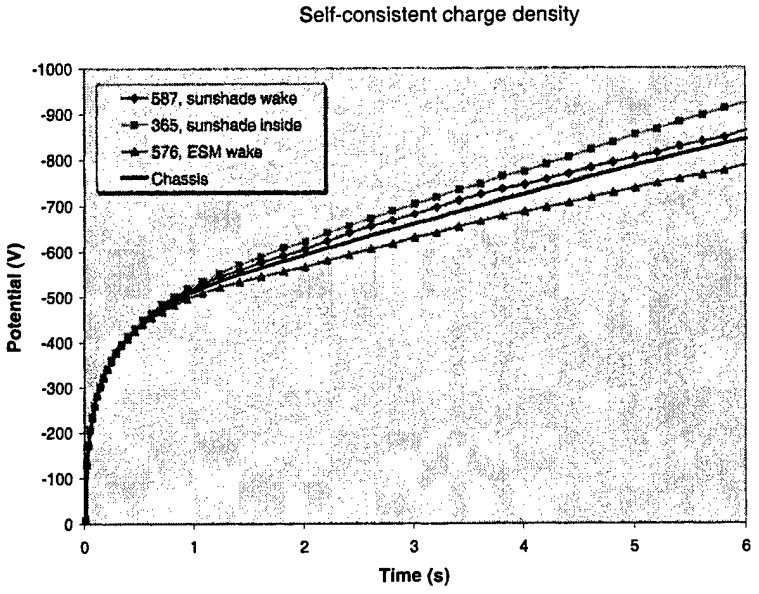

Figure 27. Time History of Charging with Self-Consistent Charge Density.

Several interesting features can be seen in the space potentials. In the analytic space charge case, the potentials follow the contours of the satellite more closely and the influence of the wake in the higher potential regions is more pronounced. In the self-consistent space charge case, the potential falls off a bit faster in the wake, and the sheath edge is much smoother on the ram side.

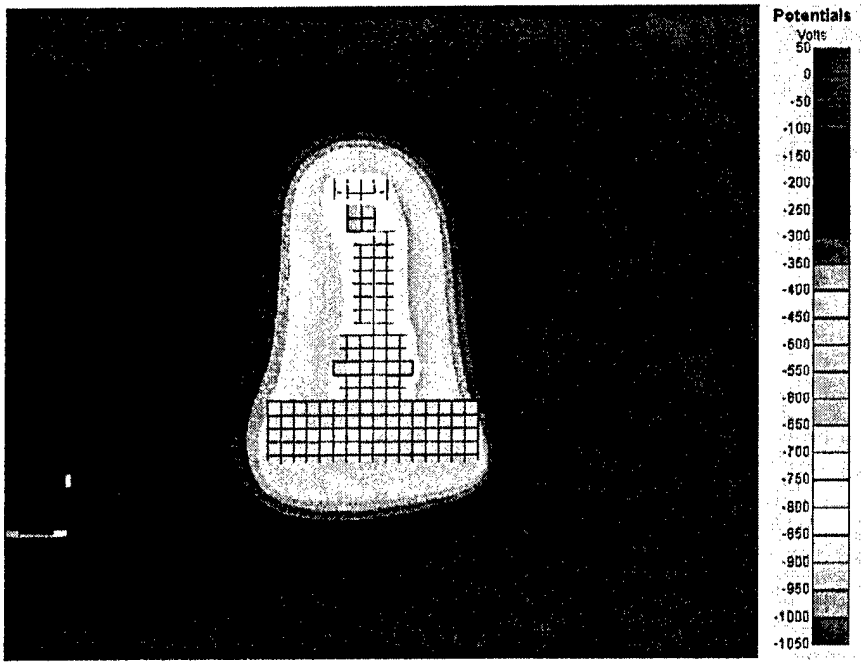

Figure 28. Resulting Space Potentials for Case with Analytic Charge Density.

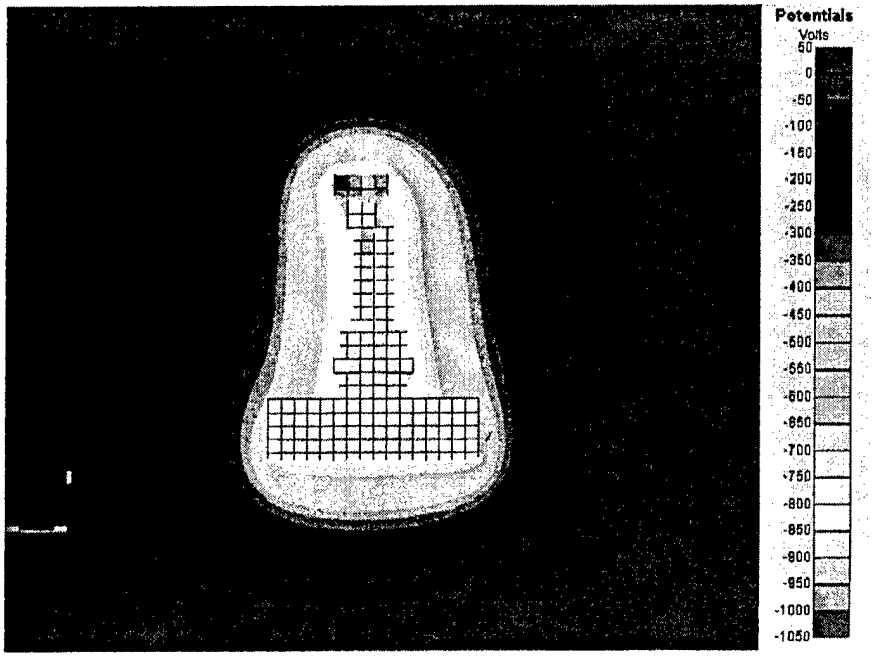

Figure 29. Resulting Space Potentials for Case with Self-Consistent Charge Density.

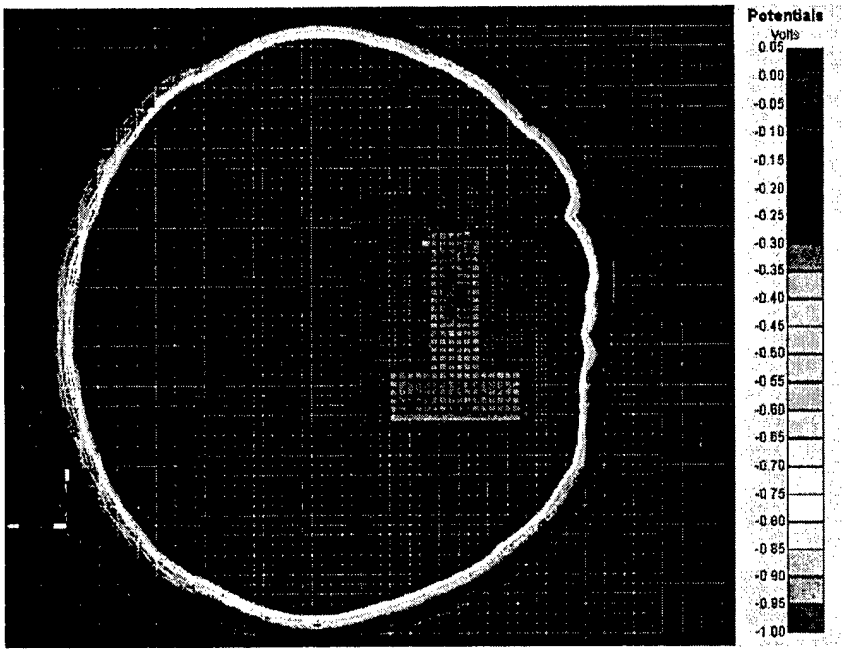

Figure 30. Resulting Sheath Location for Case with Analytic Charge Density.

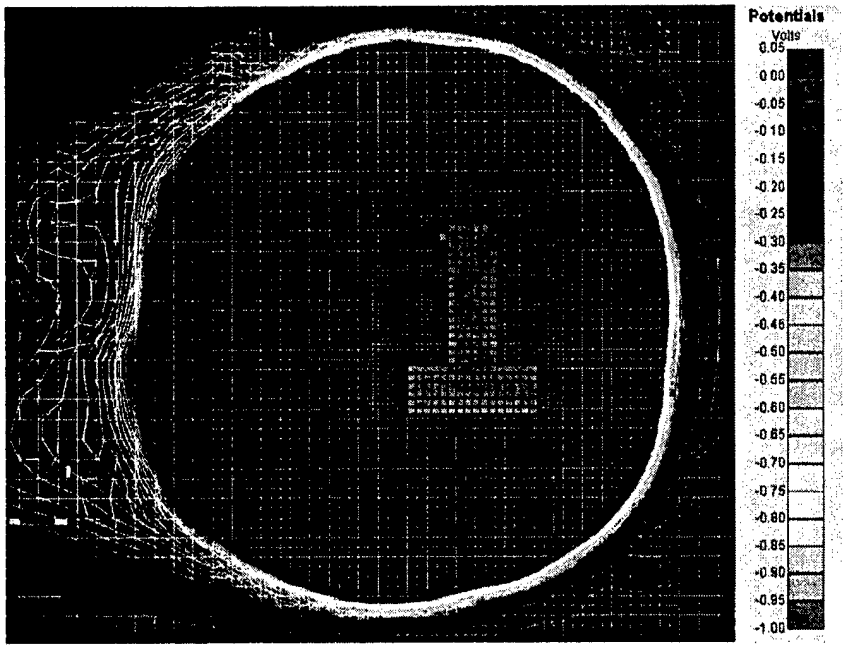

Figure 31. Resulting Sheath Location for Case with Self-Consistent Charge Density.

These results can be compared with Figure 5 of Reference 1, shown below as Figure 32. The Nascap-2k results do not have the presumably spurious hump at 0.2 sec. The Nascap-2k results show more charging and are continuing to charge. The relative charging of the different surfaces are somewhat different. As the selected surfaces are probably different, no firm conclusions can be drawn.

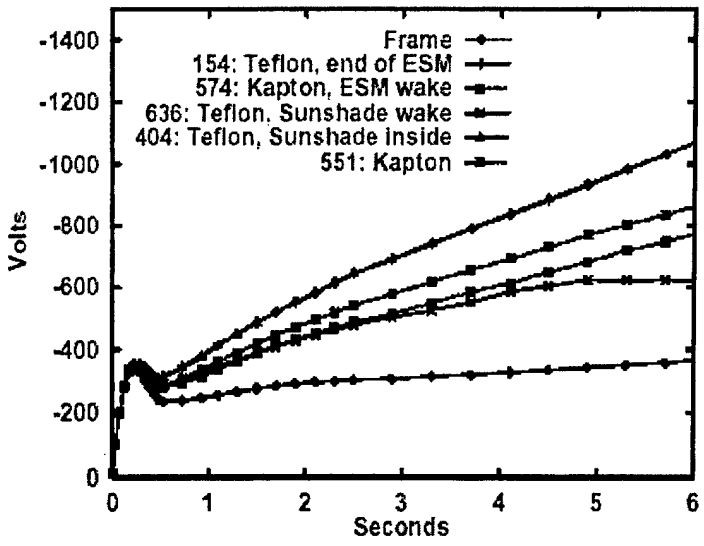

Figure 32. Figure 5 of Reference 1.

We also repeated another set calculations in the same paper. We set the thickness of Teflon to 2.8e-3 and changed all the Kapton to Teflon. The results are shown in Figure 33 through Figure 35. These results can be compared with Figure 36 through Figure 38 obtained from POLAR. Again, the results using the two codes are similar in character. The shaded surfaces are the most negative and the ram-wake difference is small. Using POLAR, the wake side charges more than the ram side. Using Nascap-2k, the ram side charges slightly more than the wake side. The incident ions are focused onto the wake side of the spacecraft.

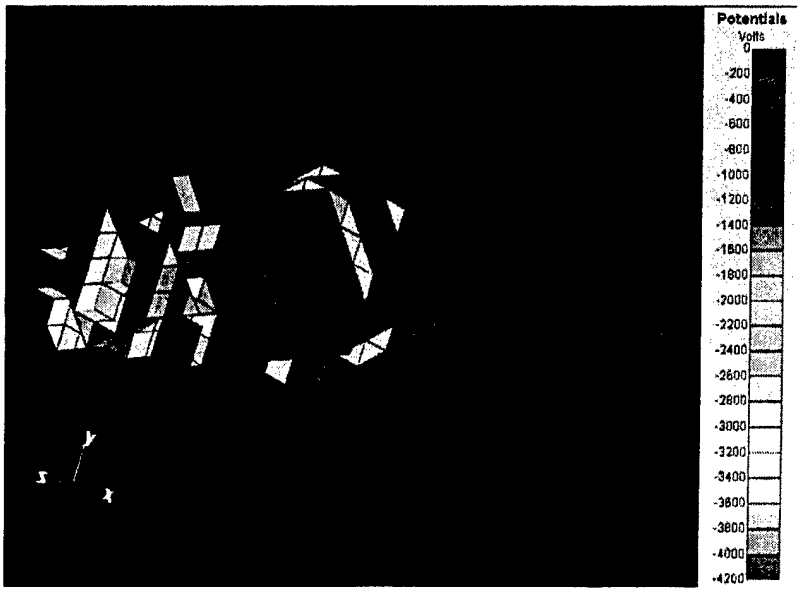

Figure 33. Resulting Surface Potentials for Case with All Teflon and Self-Consistent Charge Density.

Figure 34. Resulting Surface Potentials for Case with All Teflon and Self-Consistent Charge Density.

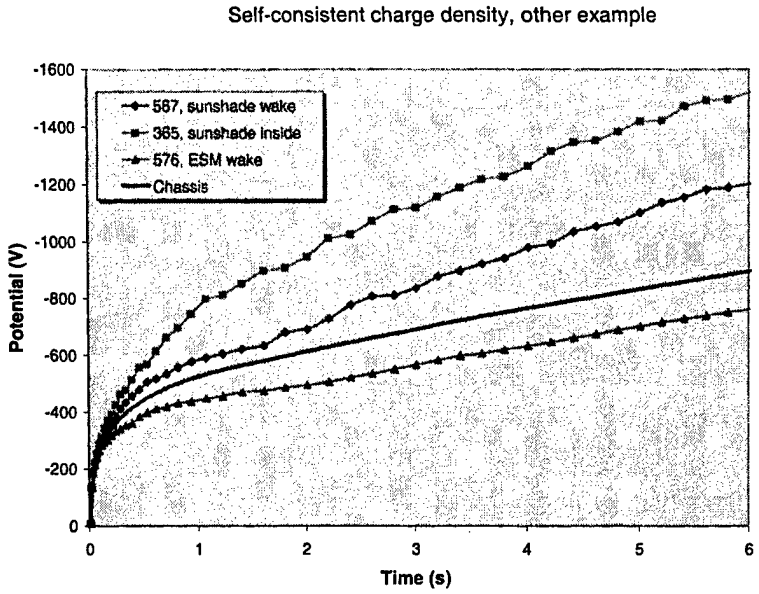

Figure 35. Time History of Charging with All Teflon and Self-Consistent Charge Density.

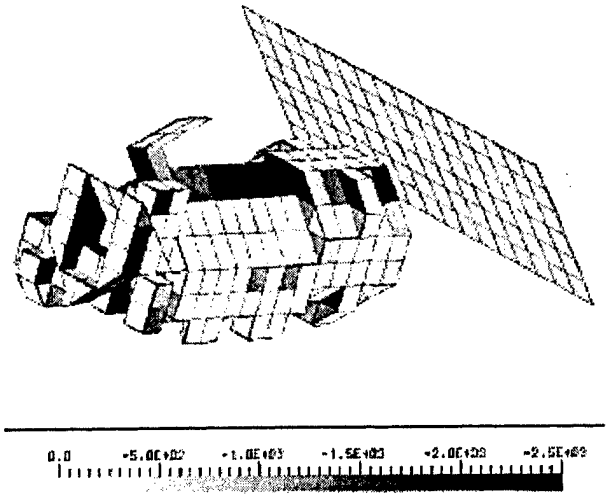

Figure 36. Resulting Surface Potentials Using POLAR for Teflon Only Case From Reference 1.

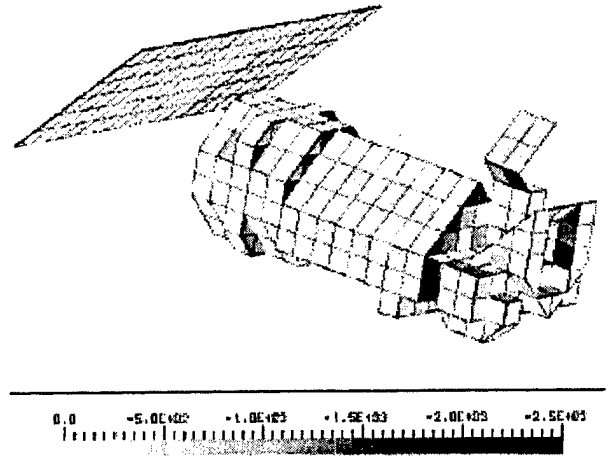

Figure 37. Resulting Surface Potentials Using POLAR for Teflon Only Case From Reference 1.

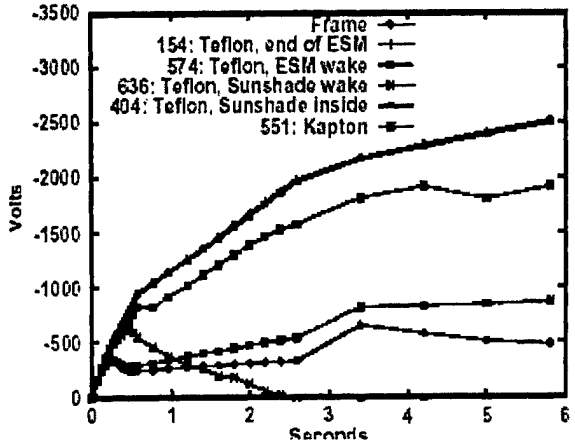

Figure 38. Time History of Surface Potentials Using POLAR for Teflon Only Case From Reference 1.

REFERENCES

D.L. Cooke, 2000, Simulation of an Auroral Charging Anomaly on the DMSP Satellite, 6th Spacecraft Charging Technology Conference, AFRL-VS-TR-2000-1578.